Electrochemical Kinetic Investigations of the Reactions of [FeFe]-Hydrogenases with Carbon Monoxide and Oxygen: Comparing the Importance of Gas Tunnels and Active-Site Electronic/R...

ARTICLE *in* JOURNAL OF THE AMERICAN CHEMICAL SOCIETY · OCTOBER 2009

Impact Factor: 12.11 · DOI: 10.1021/ja905388j · Source: PubMed

7 AUTHORS, INCLUDING:

Sven Timo Stripp
Freie Universität Berlin
18 PUBLICATIONS **511** CITATIONS
SEE PROFILE

Christine Cavazza
Atomic Energy and Alternative Energies Co...
48 PUBLICATIONS **2,332** CITATIONS
SEE PROFILE

J|A|C|S ARTICLES

Published on Web 09/22/2009

Electrochemical Kinetic Investigations of the Reactions of [FeFe]-Hydrogenases with Carbon Monoxide and Oxygen: Comparing the Importance of Gas Tunnels and Active-Site Electronic/Redox Effects

Gabrielle Goldet,[†] Caterina Brandmayr,[†] Sven T. Stripp,[‡] Thomas Happe,[‡] Christine Cavazza,[§] Juan C. Fontecilla-Camps,[§] and Fraser A. Armstrong*,[†]

Inorganic Chemistry Laboratory, Department of Chemistry, University of Oxford, South Parks Road, Oxford OX1 3QR, United Kingdom, Ruhr-Universität, Lehrstuhl fur Biochemie der Pflanzen, AG Photobiotechnologie, 44780 Bochum, Germany, and Laboratoire de Crystallographie et Crystallographie des Protéines, Institut de Biologie Structurale, J.P. Ebel, CEA, CNRS, Université Joseph Fourier, 41, rue J. Horrowitz, 38027 Grenoble Cedex 1, France

Received July 3, 2009; E-mail: fraser.armstrong@chem.ox.ac.uk

Abstract: A major obstacle for future biohydrogen production is the oxygen sensitivity of [FeFe]-hydrogenases, the highly active catalysts produced by bacteria and green algae. The reactions of three representative [FeFe]-hydrogenases with O_2 have been studied by protein film electrochemistry under conditions of both H_2 oxidation and H_2 production, using CO as a complementary probe. The hydrogenases are *Dd*HydAB and *Ca*HydA from the bacteria *Desulfovibrio desulfuricans* and *Clostridium acetobutylicum*, and *Cr*HydA1 from the green alga *Chlamydomonas reinhardtii*. Rates of inactivation depend on the redox state of the active site 'H-cluster' and on transport through the protein to reach the pocket in which the H-cluster is housed. In all cases CO reacts much faster than O_2. In the model proposed, *Ca*HydA shows the most sluggish gas transport and hence little dependence of inactivation rate on H-cluster state, whereas *Dd*HydAB shows a large dependence on H-cluster state and the least effective barrier to gas transport. All three enzymes show a similar rate of reactivation from CO inhibition, which increases upon illumination: the rate-determining step is thus assigned to cleavage of the labile Fe-CO bond, a reaction likely to be intrinsic to the atomic and electronic state of the H-cluster and less sensitive to the surrounding protein.

Introduction

The increasing need for clean, renewable fuels is stimulating new research on hydrogen (H_2) production,[1−5] and one promising solution is to exploit microorganisms in 'H_2 farms'. In biology, H_2 is evolved by metalloenzymes called hydrogenases, in processes ranging from fermentation to photosynthesis. Hydrogenases are highly efficient enzymes—so much so that when attached to an electrode, they are, like platinum, superb electrocatalysts of both H_2 oxidation and H_2 production, at or close to the reversible potential for the $2H^+/H_2$ couple.[6−8]

Of the two main classes, [NiFe]- and [FeFe]-hydrogenases, named according to the metals present in the center at which H_2 is activated, the [FeFe]-hydrogenases are considered to be more active in H_2 production.[9] However, a perceived major disadvantage of [FeFe]-hydrogenases (with respect to [NiFe]-hydrogenases) is their higher O_2 sensitivity.[10] The [NiFe]-hydrogenases react rapidly with O_2 to give inactive, EPR-characterized, Ni(III) forms that can be reactivated by reduction: Ni-A ('unready') is reactivated very slowly whereas Ni-B ('ready') can be reactivated within seconds, hence there is a rapid repair mechanism for hydrogenases that produce only Ni-B.[6,11] In contrast, the [FeFe]-hydrogenases appear to undergo irreparable damage when exposed to O_2 while in their active state (after reduction).[12−14] The incompatibility of O_2 with [FeFe]-hydrogenases poses a major limitation to progress in 'biohydrogen' production, in particular by modified photosyn-

[†] University of Oxford.
[‡] Ruhr-Universitat.
[§] Université Joseph Fourier.

(1) Navarro, R. M.; Pena, M. A.; Fierro, J. L. G. *Chem. Rev.* **2007**, *107*, 3952–3991.
(2) Mertens, R.; Liese, A. *Curr. Opin. Biotechnol.* **2004**, *15*, 343–348.
(3) Hankamer, B.; Lehr, F.; Rupprecht, J.; Mussgnug, J. H.; Posten, C.; Kruse, O. *Physiol. Plant.* **2007**, *131*, 10–21.
(4) Liu, X. M.; Ibrahim, S. K.; Tard, C.; Pickett, C. J. *Coord. Chem. Rev.* **2005**, *249*, 1641–1652.
(5) Melis, A.; Happe, T. *Plant Physiol.* **2001**, *127*, 740–748.
(6) Vincent, K. A.; Parkin, A.; Armstrong, F. A. *Chem. Rev.* **2007**, *107*, 4366–4413.
(7) Jones, A. K.; Sillery, E.; Albracht, S. P. J.; Armstrong, F. A. *Chem. Commun.* **2002**, 866–867.
(8) Hambourger, M.; Gervaldo, M.; Svedruzic, D.; King, P. W.; Gust, D.; Ghirardi, M.; Moore, A. L.; Moore, T. A. *J. Am. Chem. Soc.* **2008**, *130*, 2015–2022.
(9) Frey, M. *ChemBioChem* **2002**, *3*, 153–160.
(10) Adams, M. W. W. *Biochim. Biophys. Acta* **1990**, *1020*, 115–145.
(11) Armstrong, F. A.; Belsey, N. A.; Cracknell, J. A.; Goldet, G.; Parkin, A.; Reisner, E.; Vincent, K. A.; Wait, A. F. *Chem. Soc. Rev.* **2009**, *38*, 36–51.
(12) Erbes, D. L.; King, D.; Gibbs, M. *Plant Physiol.* **1979**, *63*, 1138–1142.
(13) Erbes, D. L.; King, D.; Gibbs, M. *Plant Physiol.* **1978**, *61*, 23–23.
(14) Vincent, K. A.; Parkin, A.; Lenz, O.; Albracht, S. P. J.; Fontecilla-Camps, J. C.; Cammack, R.; Friedrich, B.; Armstrong, F. A. *J. Am. Chem. Soc.* **2005**, *127*, 18179–18189.

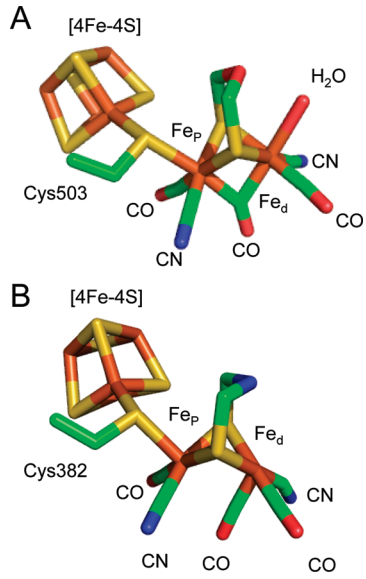

Figure 1. Structures of H-clusters of the [FeFe]-hydrogenase from *Clostridium pasteurianum* (*Cp*I) and *Desulfovibrio desulfuricans* (*Dd*HydAB) constructed using PyMol. A) *Cp*I H-cluster (PDB code: 3C8Y).[23] B) *Dd*HydAB H-cluster.[25] The two structures were modeled with different bridgehead atoms—O for *Cp*I, and N for *Dd*HydAB—but this distinction is not directly relevant for this paper.

thesis.[15] In green algae the O_2-sensitivity of the [FeFe]-hydrogenase is the bottleneck for producing H_2 from sunlight. Production of H_2 is stimulated during sulfur deprivation, conditions under which only 10% of the photosystem II remains active and the system effectively becomes anaerobic.[16] Green algae that could express an O_2-tolerant [FeFe]-hydrogenase would therefore provide much increased levels of H_2 production.[15]

The buried active site of [FeFe]-hydrogenases is actually a complex 6Fe unit known as the 'H-cluster' which contains a [4Fe-4S] subcluster (generally referred to as $[4Fe\text{-}4S]_H$) in addition to the di-iron subcluster ($2Fe_H$).[17] The two independent representations of the H-cluster shown in Figure 1 are directly relevant to the catalytically active states known as H_{ox} and H_{red} that have been extensively characterized.[18,19] General features of the structure are as follows: (a) the $[4Fe\text{-}4S]_H$ subcluster is linked to one of the Fe atoms of the $2Fe_H$ subcluster by a bridging cysteine sulfur (the Fe atoms of $2Fe_H$ are thus known as 'proximal' (Fe_p) and 'distal' (Fe_d) with respect to the $[4Fe\text{-}4S]_H$ subcluster);[20] (b) both Fe_d and Fe_p are coordinated by CO and CN^- ligands;[17] (c) an unusual SCH_2XCH_2S dithiolate ligand forms a di-μ-thiolato bridge between Fe_p and Fe_d, and although opinions differ as to whether the bridgehead atom X is an O or N atom,[21−25] recent investigations with ^{14}N HYSCORE have provided direct evidence that X = N.[21]

In the structure of H_{ox}, as determined with the *Cp*I enzyme from *Clostridium pasteurianum*, Fe_p is coordinated by one CO and one CN^- ligand and shares a bridging CO with Fe_d.[20] In turn, Fe_d is also coordinated by one CO and one CN^- ligand, and an additional binding site is vacant or occupied by an exchangeable O-ligand, most likely a water molecule (Figure 1A). In the structure of the [FeFe]-hydrogenase from *Desulfovibrio desulfuricans*, which should be in the H_{red} form, the bridging CO is replaced by a terminal CO on Fe_d (Figure 1B).[26] Recent EPR spectroscopic investigations favor an oxidation state assignment of $[4Fe\text{-}4S]^{2+}$-$Fe_p(I)Fe_d(II)$ for H_{ox}, with some spin density delocalized onto the $[4Fe\text{-}4S]_H$ subcluster,[27] although H-clusters from different enzymes show minor variations in electronic structure.[28] The EPR-silent H_{red} state is assigned as $[4Fe\text{-}4S]^{2+}$-Fe(I)Fe(I) which, if protonated, is formally equivalent to the hydrido species $[4Fe\text{-}4S]^{2+}$-Fe(II)Fe(II)-H^-.[17] As also determined by EPR spectroscopy, exogenous CO, a competitive inhibitor of H_2 oxidation, reacts with H_{ox}.[29] Crystallographic and infrared spectroscopic studies of H_{ox}-CO further show that binding of CO (which is photolabile) occurs at Fe_d.[30−33] Inactivation by anaerobic oxidants gives rise to a form known as H_{ox}^{inact}, usually formulated as $[4Fe\text{-}4S]^{2+}$-Fe(II)Fe(II), which can be reactivated upon reduction—a process occurring via an intermediate known as H_{trans} which has been formulated as $[4Fe\text{-}4S]^{+}$-Fe(II)Fe(II), i.e. with the $[4Fe\text{-}4S]_H$ subcluster reduced.[33] The H-cluster is remarkable among non-macrocycle cofactors because the $2Fe_H$ subcluster at which H_2 is produced is connected to the protein through just a half-share of a cysteine sulfur: it is very much an organometallic-like compound physically enclosed in protein.

Despite these intense studies by crystallography and spectroscopy, numerous aspects of the reactions of [FeFe]-hydrogenases remain unresolved. These aspects include the activation process (there is evidence from electrochemical titrations that a two-electron process is also involved)[33] and many details of the mechanism of catalysis in either direction, including the exact function of the $[4Fe\text{-}4S]_H$ subcluster. The nature and products of the degradation by O_2 are only now coming to light,[34] and a major issue is whether and how H_2 production could be sustainable at all in the presence of O_2.

This article describes mechanistic investigations, by protein film electrochemistry, of the O_2 inactivation kinetics of three representative [FeFe]-hydrogenases. These are: the hydrogenase

(15) Ghirardi, M. L.; Posewitz, M. C.; Maness, P.-C.; Dubini, A.; Yu, J.; Seibert, M. *Annu. Rev. Plant Biol.* **2007**, *58*, 71–91.
(16) Hemschemeier, A.; Fouchard, S.; Cournac, L.; Peltier, G.; Happe, T. *Planta* **2008**, *227*, 397–407.
(17) Fontecilla-Camps, J. C.; Volbeda, A.; Cavazza, C.; Nicolet, Y. *Chem. Rev.* **2007**, *107*, 4273–4303.
(18) Lubitz, W.; Reijerse, E.; van Gastel, M. *Chem. Rev.* **2007**, *107*, 4331–4365.
(19) De Lacey, A. L.; Fernandez, V. M.; Rousset, M.; Cammack, R. *Chem. Rev.* **2007**, *107*, 4304–4330.
(20) Nicolet, Y.; Lemon, B. J.; Fontecilla-Camps, J. C.; Peters, J. W. *Trends Biochem. Sci.* **2000**, *25*, 138–143.
(21) Silakov, A.; Wenk, B.; Reijerse, E.; Lubitz, W. *Phys. Chem. Chem. Phys.* **2009**, *11*, 6592–9.
(22) Peters, J. W.; Lanzilotta, W. N.; Lemon, B. J.; Seefeldt, L. C. *Science* **1998**, *282*, 1853–1858.
(23) Pandey, A. S.; Harris, T. V.; Giles, L. J.; Peters, J. W.; Szilagyi, R. K. *J. Am. Chem. Soc.* **2008**, *130*, 4533–4540.
(24) Barton, B. E.; Olsen, M. T.; Rauchfuss, T. B. *J. Am. Chem. Soc.* **2008**, *130*, 16834–5.
(25) Nicolet, Y.; De Lacey, A. L.; Vernede, X.; Fernandez, V. M.; Hatchikian, E. C.; Fontecilla-Camps, J. C. *J. Am. Chem. Soc.* **2001**, *123*, 1596–1601.
(26) Nicolet, Y.; Piras, C.; Legrand, P.; Hatchikian, C.; Fontecilla-Camps, J. C. *Structure* **1999**, *7*, 13–23.
(27) Silakov, A.; Reijerse, E. J.; Albracht, S. P. J.; Hatchikian, E. C.; Lubitz, W. *J. Am. Chem. Soc.* **2007**, *129*, 11447–11458.
(28) Kamp, C.; Silakov, A.; Winkler, M.; Reijerse, E. J.; Lubitz, W.; Happe, T. *Biochim. Biophys. Acta* **2008**, *1777*, 410–416.
(29) Bennett, B.; Lemon, B. J.; Peters, J. W. *Biochemistry* **2000**, *39*, 7455–7460.
(30) Lemon, B. J.; Peters, J. W. *J. Am. Chem. Soc.* **2000**, *122*, 3793–3794.
(31) Lemon, B. J.; Peters, J. W. *Biochemistry* **1999**, *38*, 12969–12973.
(32) De Lacey, A. L.; Stadler, C.; Cavazza, C.; Hatchikian, C.; Fernandez, V. M. *J. Am. Chem. Soc.* **2000**, *122*, 11232–11233.
(33) Roseboom, W.; Lacey, A. L.; Fernandez, V. M.; Hatchikian, E. C.; Albracht, S. P. J. *J. Biol. Inorg. Chem.* **2006**, *11*, 102–118.
(34) Stripp, S.; Goldet, G.; C., B.; Vincent, K. A.; Armstrong, F. A.; Happe, T. *Proc. Natl. Acad. Sci. U.S.A.* **2009**, in press.

from a sulfate-reducing bacterium, *Desulfovibrio desulfuricans*, abbreviated as *Dd*HydAB which has been crystallographically characterized;[26] the hydrogenase from *Clostridium acetobutylicum*, abbreviated as *Ca*HydA, which is potentially of importance for H_2 production by anaerobic fermentation and has high sequence similarity with the crystallographically characterized *Cp*I hydrogenase from *C. pasteurianum*,[22] and the hydrogenase known as *Cr*HydA1 from the green alga *Chlamydomonas reinhardtii*, which is of interest for photosynthetic H_2 production.[35] Both *Dd*HydAB and *Ca*HydA contain a series of Fe−S clusters[17] to relay electrons within the protein for transfer to and from the redox partner (in our case the electrode); in contrast *Cr*HydA1 possesses no Fe−S clusters apart from the $[4Fe\text{-}4S]_H$ subcluster,[36,37] but it is nonetheless electrocatalytically active when adsorbed on an electrode.[34] Although the three enzymes differ in their overall tertiary and quaternary structures, their H-domains that house the H-cluster are very similar.[17]

In protein film electrochemistry, an enzyme is immobilized on the surface of an electrode such that its properties are controlled directly by the electrode potential.[6,38] Catalytic activity in either direction, oxidation or reduction, can be driven and recorded at any particular potential value and the catalytic rate is directly proportional to the current that flows. Various gas mixtures (produced by mass-flow controllers) can be introduced and flushed from the sealed electrochemical cell in which the electrode is rotated rapidly to provide precise hydrodynamic control (supply of reactants and removal of products). A particular advantage of this approach is that turnover activity in either direction is immediately and directly observed from the catalytic current; thus, *rates of change* of activity, such as those induced by CO or O_2, are extracted directly from the variation of current with time, all as a precise function of the electrode potential. In this way, extremely complex reactivities become resolvable; therefore, this technique both complements and instigates structural and spectroscopic investigations.

We first establish, for each enzyme, how H_2 oxidation and H_2 production are affected by the concentrations of H_2 and CO; next we examine the kinetics of CO binding and release and correlate these data with equilibrium values; we then examine the kinetics of O_2 inactivation of H_2 oxidation activity; finally, we exploit CO inhibition as a tool to investigate H_2 production in the presence of O_2. Recent studies have established that CO is able to protect [FeFe]-hydrogenases against inactivation by O_2,[34,39] an observation suggesting that the sequence of destruction is initiated by O_2 coordinating to the same site at which exogenous CO binds, i.e. Fe_d.[30−33] Thereafter, the mechanism remains less clear, but recent EXAFS evidence obtained with *Cr*HydA1 shows that the $[4Fe\text{-}4S]_H$ subcluster is altered more than the $2Fe_H$ subcluster.[34] Our experiments show clearly how the destructive power of O_2 varies among the hydrogenases with an interesting dependence on catalytic direction (H_2 oxidation compared to H_2 production)—thus implicating sensitivity to the oxidation level of the active site. The results provide insight for the quest for solutions to the oxygen problem in biohydrogen production by photosynthesis. The functional differences between the [FeFe]-hydrogenases are not immediately evident from the structures that have been obtained for *Dd*HydAB and *Cp*1.

Methods

Previously reported protocols were employed to obtain pure samples of *Dd*HydAB,[40] *Cr*HydA1 and *Ca*HydA.[41] In each case levels of CO, O_2 and H_2 present during cell growth were extremely low. Protein film electrochemistry experiments were carried out in an anaerobic glovebox (M Braun) comprising a N_2 atmosphere. The solutions contained 0.05 M phosphate buffer with 0.10 M NaCl as additional supporting electrolyte, and were prepared using standard reagents NaCl, NaH_2PO_4 and Na_2HPO_4 (Analytical Reagent grade, Sigma) in purified water (Millipore 18 MΩ cm). The working electrode was a disk (area 0.03 cm^2) of pyrolytic graphite oriented so that the 'edge plane' faced the solution. This is called a pyrolytic graphite edge (PGE) electrode and it was used in conjunction with an electrode rotator (EcoChemie) that fitted snugly into a specially designed, gastight, glass electrochemical cell. The cell featured a water jacket for temperature control. Due to the light sensitivity of [FeFe]-hydrogenases the entire surface of the cell was blacked-out with adhesive masking tape. In experiments to detect photolabilization, the tape at the bottom of the cell was removed to allow illumination from a 150 W lamp placed just beneath the cell (see Figure SI.1, Supporting Information). A saturated calomel reference electrode (SCE) was placed in a side arm containing 0.1 M NaCl, connected to the main cell compartment by a Luggin capillary. A Pt wire was used as the counter electrode. Potentials (E) are quoted with respect to the standard hydrogen electrode (SHE) using the correction $E_{SHE} = E_{SCE} + 242$ mV at 298 K.[42] Electrochemical experiments were performed using an electrochemical analyzer (Autolab PGSTAT10 or 20) controlled by a computer operating GPES software (EcoChemie). Mass flow controllers (Smart-Trak Series 100, Sierra Instruments, U.S.A.) were used to prepare precise gas mixtures (headspace fractions accurate to within 1%) and to impose constant gas flow rates into the electrochemical cell during experiments. Gases used were H_2 (Premier grade, Air Products), O_2 (Air Products), CO (Research grade, BOC), 1% CO in N_2 (Research grade, BOC), N_2 (Oxygen-free, BOC) or mixtures of these gases. Henry's law was applied to estimate the concentration of gas in solution in each experiment.[43] Values taken for use at 10 °C were: 100% CO, 1248 μM; 100% O_2, 1624 μM.

To prepare each enzyme film, the PGE electrode was first polished for 10 s with an aqueous slurry of α-alumina (1 μm, Buehler) and sonicated for 5 s in purified water, before enzyme solution (1.5 μL, containing 0.015−0.15 μg, pH 8) was applied and removed after a few minutes. The electrode was then placed in enzyme-free buffered electrolyte so that the only enzyme molecules being addressed were on the electrode and subjected to the same regime of strict potential control. In all experiments the electrode was rotated at a constant high rate (3000−5000 rpm) to ensure efficient supply of substrate and removal of product.

In experiments measuring the effect of O_2 on hydrogenase-catalyzed H_2 production, it was necessary to estimate the concentration of O_2 that the enzyme molecules at the electrode surface actually experience, given that a portion of the total dissolved O_2 is consumed by the electrode at this potential (−0.4 V). Using a

(35) Ghirardi, M. L.; Dubini, A.; Yu, J. P.; Maness, P. C. *Chem. Soc. Rev.* **2009**, *38*, 52–61.
(36) Stripp, S.; Sanganas, O.; Happe, T.; Haumann, M. *Biochemistry* **2009**, *48*, 5042–5049.
(37) Happe, T.; Naber, J. D. *Eur. J. Biochem.* **1993**, *214*, 475–481.
(38) Léger, C.; Bertrand, P. *Chem. Rev.* **2008**, *108*, 2379–2438.
(39) Baffert, C.; Demuez, M.; Cournac, L.; Burlat, B.; Guigliarelli, B.; Bertrand, P.; Girbal, L.; Leger, C. *Angew. Chem., Int. Ed.* **2008**, *47*, 2052–2054.
(40) Hatchikian, C.; Forget, N.; Fernandez, V. M.; Williams, R.; Cammack, R. *Eur. J. Biochem.* **1992**, *209*, 357–365.
(41) von Abendroth, G.; Stripp, S.; Silakov, A.; Croux, C.; Soucaille, P.; Girbal, L.; Happe, T. *Int. J. Hydrogen Energy* **2008**, *33*, 6076–6081.
(42) Bard, A. J.; Faulkner, L. R. *Electrochemical Methods. Fundamentals and Applications*, 2nd ed.; Wiley: New York, 2001.
(43) Sander, R. http://www.henrys-law.org, 1999.

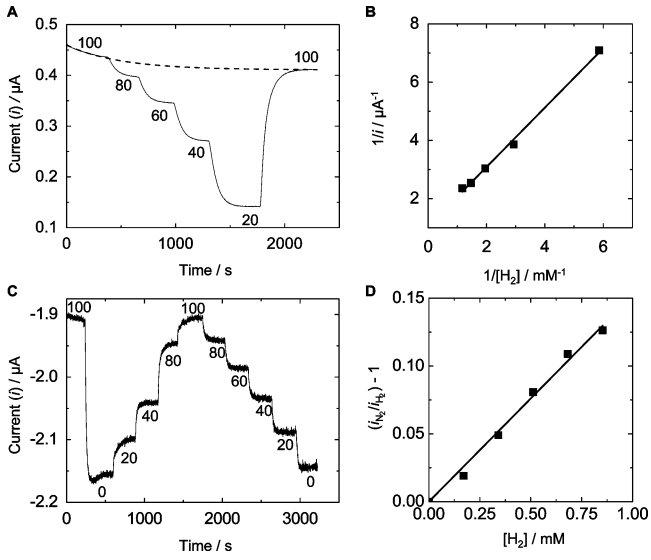

Figure 2. Determination of $K_M^{H_2}$ (A and B) and K_I^{app} (C and D) for *Ca*HydA. (Panel A) chronoamperometric experiment performed at −0.05 V, at pH 6, 10 °C. The broken line traces the progression of film loss throughout the experiment. (Panel B) Lineweaver−Burk plot from experiment shown in A fitted to a straight line. (Panel C) chronoamperometric experiment performed to determine K_I^{app} at −0.4 V, at pH 6.0, 10 °C. The concentration of H_2 in N_2 (%) in the headspace of the cell is indicated. The rotation rate was varied from 3000 to 4000 and 5000 rpm at each concentration of H_2 to ensure that inhibition was not mass-transport limited. (Panel D) Plot according to the procedure described by Léger et al.[45] from which K_I^{app} is determined, showing the line of best fit.

previously published method,[44] it was estimated that 0.7% O_2 (11 μM in solution at 10 °C) survives to be experienced by the enzyme when 1% O_2 is flowed through the headspace of the cell and 4.5% (73 μM) survives when 5% O_2 is used.

Results

Measurements of the H_2 Concentration Dependencies for H_2 Oxidation and Production. We first evaluated the affinity of the enzymes for H_2 both in terms of K_M for H_2 as the substrate in H_2 oxidation ($K_M^{H_2}$) and the apparent inhibition constant K_I^{app} for H_2 as the product inhibitor of H^+ reduction. Figure 2 shows experiments carried out for *Ca*HydA: analogous experiments were carried out for *Cr*HydA1, but films of *Dd*HydAB were not sufficiently stable to obtain accurate measurements over the period of time required (30−60 min.). Experiments to determine $K_M^{H_2}$ were conducted by varying the ratio of H_2 to N_2 in the headgas and measuring the oxidation current after allowing time for the gas mixture to equilibrate with the cell solution at each concentration of H_2 (Figure 2A). The experiments were performed at an electrode potential of −0.05 V to avoid the anaerobic inactivation that occurs at higher potential (see Figure 3). We and others, have noted that K_M and K_I are potential-dependent quantities,[44,45] and the potential must therefore be specified. It was also important to make measurements under conditions where the current was limited by the catalytic rate of the enzyme rather than by mass transport of substrate to (or product from) the electrode. The experiments were therefore carried out at low temperature (10 °C) to decrease the rate of catalysis. The low temperature also minimized the rate of film loss. At each H_2 concentration the electrode rotation rate was stepped between 3000 and 5000 rpm to ensure that the current (and thus the rate of reaction) was independent of rotation rate. Values of $K_M^{H_2}$ were calculated from the *x*-intercept of the Lineweaver−Burk plot shown in Figure 2B and are summarized in Table 1. Experiments to measure the apparent inhibition constant (K_I^{app}, defined in eq 1 where $K_M^{H^+}$ is the K_M

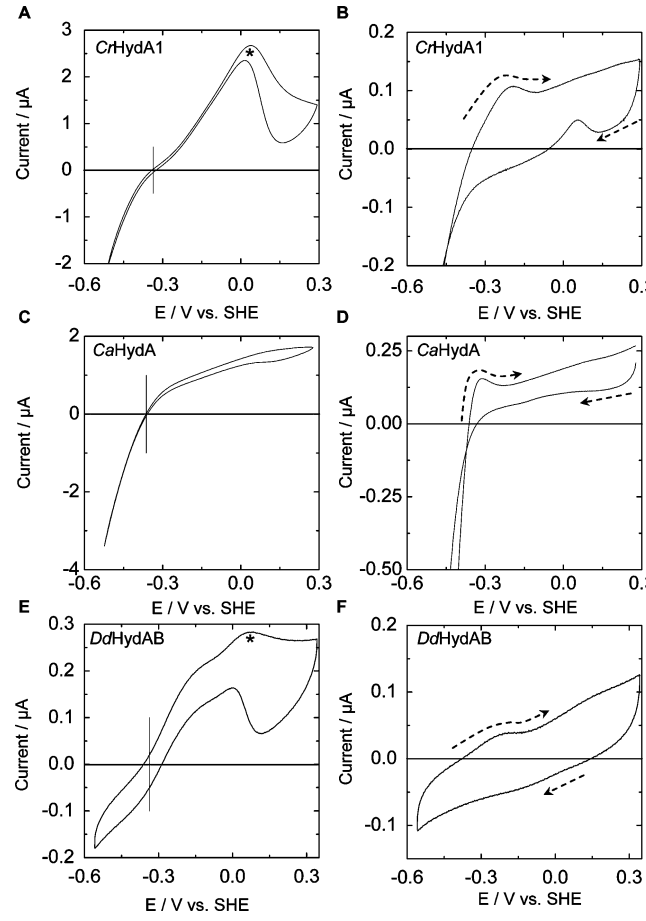

Figure 3. Cyclic voltammograms showing bidirectional electrocatalytic H^+ reduction and H_2 oxidation by *Cr*HydA1 (A), *Ca*HydA (C) and *Dd*HydAB (E) at pH 6.0 under 1 bar H_2. Panels B, D, F show the time-dependent voltammograms recorded following introduction of CO, introduced prior to the scans shown here, as the potential was being cycled between −0.55 V and +0.3 V, as it is removed from the cell: these reveal different reactions as CO dissociates and rebinds as a function of potential. Experimental conditions for *Cr*HydA1: 10 °C, scan rate 20 mV/s, inhibition was achieved by injection of CO-saturated buffer to give an immediate concentration of 100 μM CO in solution 5 min prior to the scan shown in panel B. Experimental conditions for *Ca*HydA: 32 °C, electrode rotation 3000 rpm, scan rate 20 mV/s, inhibition was achieved by flushing 100% CO through the cell 5 min prior to the scan shown in panel D. Experimental conditions for *Dd*HydAB: 10 °C, electrode rotation 3000 rpm, scan rate 10 mV/s, inhibition was achieved by injection of CO-saturated buffer to give an instant concentration of 30 μM CO in solution 5 min prior to the scan shown in panel F. The dashed arrows indicate the direction of scanning. The asterisks (*) indicate the potential above which anaerobic inactivation takes place for *Cr*HydA1 and *Dd*HydAB.

Table 1. Values of $K_M^{H_2}$ and K_I^{app} for *Cr*HydA1 and *Ca*HydA Determined at pH 6, 10 °C from the Experiments Shown in Figure 2[a]

enzyme	$K_M^{H_2}$/mM	K_I^{app}/ mM
*Cr*HydA1	0.19 ± 0.03	3.7 ± 0.6
*Ca*HydA	0.46 ± 0.06	6.2 ± 1.1

[a] $K_M^{H_2}$ and K_I^{app} were calculated at −0.05 and −0.4 V, respectively.

(44) Goldet, G.; Wait, A. F.; Cracknell, J. A.; Vincent, K. A.; Ludwig, M.; Lenz, O.; Friedrich, B.; Armstrong, F. A. *J. Am. Chem. Soc.* **2008**, *130*, 11106–11113.
(45) Léger, C.; Dementin, S.; Bertrand, P.; Rousset, M.; Guigliarelli, B. *J. Am. Chem. Soc.* **2004**, *126*, 12162–12172.

for binding of the substrate H^+ and K_I is the real inhibition constant) were conducted at −0.4 V vs SHE using a similar experimental method (Figure 2C). Values of K_I^{app} were calculated by adapting the method based on that reported by Léger et al.[45] which requires plotting the data according to eq 2 (in which i_{N_2} is the current recorded under 100% N_2 and i_{H_2} is the current recorded at each concentration of H_2) as shown in Figure 2D. The K_I^{app} values are included in Table 1.

$$K_I^{app} = \frac{K_I[H^+]}{K_M^{H^+}}\left(1 + \frac{K_M^{H^+}}{[H^+]}\right) \quad (1)$$

$$(i_{N_2}/i_{H_2}) - 1 = \frac{[H_2]}{K_I^{app}} \quad (2)$$

The $K_M^{H_2}$ values are much higher than those we have measured recently for some O_2-tolerant [NiFe]-hydrogenases[46] and they suggest that the catalytic current for H_2 oxidation will be sensitive to changes in H_2 levels even close to 1 bar partial pressure (this is particularly so for *Ca*HydA). The results showed that headspace H_2 levels should be maintained constant in quantitative H_2 oxidation experiments. In contrast, the K_I^{app} values are so high that the presence of H_2 is not expected to pose a problem in studies of H_2 production. The order of magnitude difference between K_I^{app} and $K_M^{H_2}$ suggests immediately that the electronic/catalytic state of the H-cluster exerts a strong effect on binding affinity, with H_2 binding more weakly to a more reduced state.

Reactions with CO. Cyclic voltammograms of the electrocatalytic activities of *Dd*HydAB, *Cr*HydA1 and *Ca*HydA at pH 6.0 under a flow of 100% H_2 are shown in Figure 3 (A, C, E—left-hand column). These voltammograms show that all the enzymes are bidirectional, with *Ca*HydA being particularly biased in the direction of H_2 production. The traces in either potential direction cut through the zero current axis at the cell potential (see vertical line) for the $2H^+/H_2$ couple. At high potentials, all three enzymes undergo inactivation to give a species that is most likely H_{ox}^{inact} although this process is very slow for *Ca*HydA. The voltammograms in the right-hand column (B, D, F) were recorded during the efflux of CO that had been introduced by injecting a saturated solution (giving a concentration of 100 μM CO in the cell for the experiment on *Cr*HydA1, 30 μM for the experiment on *Dd*HydAB) or flowing 100% CO briefly through the cell (for *Ca*HydA) as the potential was cycled between −0.55 and 0 V prior to the scans shown in panels B, D, and F.

Informative changes in the voltammograms of *Dd*HydAB, *Cr*HydA1 and *Ca*HydA occur upon removal of CO during continuous cycling (B, D, F). In all cases the voltammograms show that once the potential is made sufficiently positive to start H_2 oxidation, there is an initial increase in current which is followed by a decrease (see the dashed arrow indicating the oxidative sweep). The magnitude of this effect is most apparent after a certain time has elapsed, dependent upon the hydrogenase, and finally the voltammograms resume the expected shapes for H_2 oxidation and production at pH 6 under 1 bar H_2, analogous to those shown in the left-hand column. This cyclic 'inhibitor-on/inhibitor-off' behavior shows that CO binding to the active site is favorable and fast during H_2 oxidation but relatively weak during H_2 production. Thus CO reinhibits strongly as the potential is raised to oxidize H_2, which addresses a more oxidized form of the enzyme (above −0.3 V). The

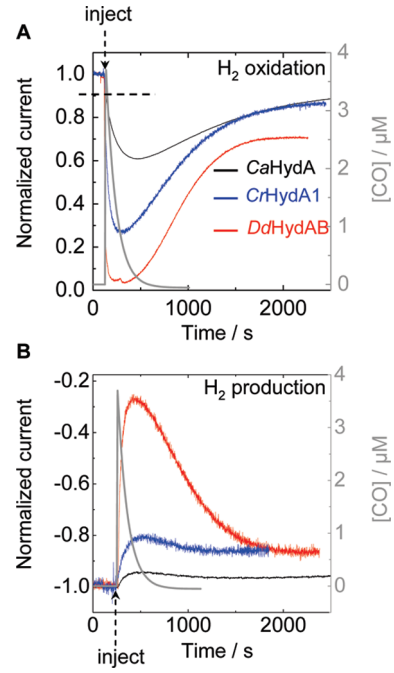

Figure 4. Inhibition of *Dd*HydAB (red lines), *Cr*HydA1 (blue lines) and *Ca*HydA (black lines) by injection of 4 μM CO at (A) −0.05 V (H_2 oxidation) and (B) −0.4 V (H_2 production). Experimental conditions: pH 6.0, 10 °C, 1 bar H_2, electrode rotation 3000 rpm. The final level of the current reached upon recovery of H_2 oxidation activity of *Ca*HydA is marked by the dashed line in A. The exponential decrease in concentration of dissolved CO is shown by the gray trace (details given in Supporting Information, Figure SI.2).

voltammogram for *Cr*HydA1 also shows an oxidation peak soon after commencing the scan in the negative direction. A similar observation was reported in previous experiments on *Dd*HydAB where it arises from the reactivation of some H_{ox}^{inact} and its rapid inactivation by CO.[47]

Further insight into CO binding and release under different conditions is provided by Figure 4. The CO inhibition profiles for *Dd*HydAB, *Cr*HydA1 and *Ca*HydA were obtained for H_2 oxidation (Panel A) or H_2 production (Panel B) by injecting an aliquot of CO-saturated solution and then recording the catalytic current as the CO is removed by flushing. The same experimental conditions (pH 6.0, 10 °C, 1 bar H_2, electrode rotation 3000 rpm) were used for all experiments. In each case, injection of CO-saturated buffer gives an immediate initial CO concentration of 4 μM which decreases exponentially to zero,[45] as depicted by the gray trace (right *y*-axis) which represents the dependence of [CO] on time throughout the experiment; < 0.2 μM CO remains in solution after 500 s. (See Supporting Information (Figure SI.2) for how this dependence is determined.) In the case of *Ca*HydA, inhibition continues to increase even though most of the CO has been flushed out of the cell, indicating that the rate of reaction with CO is slow. For H_2 oxidation, the rates and extent of inhibition reached after CO injection decrease in the order *Dd*HydAB > *Cr*HydA1 > *Ca*HydA. The reactivation rates are slow and strikingly similar for all enzymes. For H_2 production (panel B) the rates and extent of inhibition by CO again decrease in the order *Dd*HydAB > *Cr*HydA1 > *Ca*HydA.

(46) Ludwig, M.; Cracknell, J. A.; Vincent, K. A.; Armstrong, F. A.; Lenz, O. *J. Biol. Chem.* **2009**, *284*, 465–477.
(47) Parkin, A.; Cavazza, C.; Fontecilla-Camps, J. C.; Armstrong, F. A. *J. Am. Chem. Soc.* **2006**, *128*, 16808–16815.

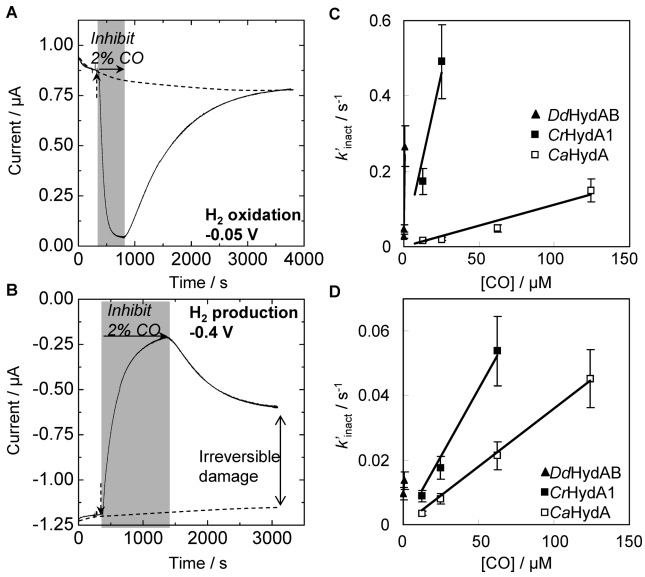

Figure 5. Inhibition by CO and reactivation, observed for H_2 oxidation and H_2 production with *Dd*HydAB, *Cr*HydA1 and *Ca*HydA. Panels A and B show experiments performed on *Ca*HydA at −0.05 and −0.4 V, respectively, in which the headgas is 80% H_2, 20% N_2 at the start of the experiment. Carbon monoxide (2%, approximately 25 μM) was introduced by injection of CO-saturated buffer (0.5 mL of buffer saturated with 10% CO, 80% H_2, 10% N_2) into the 2 mL of buffer already present in the cell and, simultaneously, flushing the headspace with 80%H_2, 18% N_2, 2% CO for the period of time marked by the gray boxes. Experimental conditions: pH 6.0, electrode rotation 3000 rpm, potentials as indicated. Panels C and D show the dependencies of rates (k'_{inact}) on CO concentration; data are derived from experiments such as those shown in panels A and B, respectively, for *Dd*HydAB, *Cr*HydA1 and *Ca*HydA.

To obtain the kinetics of CO binding for the three [FeFe]-hydrogenases it was necessary to maintain a constant CO concentration throughout the time scale of the reaction. This was achieved by injecting an aliquot of solution containing CO and simultaneously changing the gas composition reaching the headspace by replacing, with CO, a certain fraction of the 20% N_2 component of the 80% H_2 mixture. Exemplary results obtained with *Ca*HydA are shown in Figure 5. Panel A shows the time-course for CO inhibition of H_2 oxidation at −0.05 V, and Panel B shows the same time-course for inhibition of H^+ reduction at −0.4 V. Both experiments commenced with the hydrogenase on the electrode being exposed to an atmosphere of 80% H_2, 20% N_2. At $t = 300$ s, an aliquot of CO-containing solution was injected to take the cell concentration to 2% CO, and the cell was flushed with 80% H_2, 18% N_2, 2% CO. Once the catalytic current had decreased to a steady level, the CO was removed from the cell by flushing with 80% H_2, 20% N_2. (Note that 80% H_2 remained in the headspace of the cell throughout the experiment. This excludes variations in catalytic current resulting simply from changes on H_2 concentration, which would otherwise pose a problem, given the high K_M of these enzymes as indicated in Panel 1.) Pseudo first-order rate constants (k'_{inact}) were determined for each experiment from the slope of plots of ln(i) vs t, with linearity generally exceeding 75% for H_2 oxidation, although less so for H_2 production. Panels C and D show the corresponding dependencies of k'_{inact} on CO concentration, obtained for *Dd*HydAB, *Cr*HydA1 and *Ca*HydA by numerous experiments conducted analogously to those shown in panels A and B.

Values for the equilibrium inhibition constant K_I^{CO}(equil) were determined for *Cr*HydA1 and *Ca*HydA by measuring the H_2 oxidation current stabilized at different concentrations of CO. The term K_I^{CO}(equil) depends on H_2 concentration and potential, but we kept these variables constant (80% H_2, −0.05 V). These titrations were similar in design to those shown in Figure 2C and are described in more detail in Supporting Information (Figure SI.3). Values of K_I^{CO}(equil) are shown in Table 2. Comparable data for *Dd*HydAB could not be obtained because the enzyme was fully inhibited at the lowest practical CO concentrations.

Panel B of Figure 5 shows that CO inhibition of H_2 production of these enzymes is only partially reversible. This observation was consistently made with *Ca*HydA and *Cr*HydA1 but the instability of *Dd*HydAB films prevented us from making similar measurements with this enzyme. By comparison, CO inhibition is fully reversible when measuring H_2 oxidation at −0.05 V. In all cases, the background decrease in current that we refer to as film loss (traced by the dashed line) was checked through control experiments carried out without introducing CO. The rates determined for the inactivation of H_2 production by CO are therefore approximate. The potential dependence of the rate of inactivation of H_2 production was not investigated further, although we noted that the inactivation process became noticeably biphasic as the potential was lowered below −0.4 V. We raise this issue later in the Discussion.

Panels C and D of Figure 5 show that: (i) *Dd*HydAB is always the fastest to react with CO and *Ca*HydA the slowest, and ii) for all three enzymes, inhibition of H_2 oxidation measured at −0.05 V is substantially faster than inhibition of H_2 production at −0.4 V, but the same order *Dd*HydAB > *Cr*HydA1 > *Ca*HydA is observed in both catalytic directions. The second-order rate constants (k_{inact}) are provided in Table 2 (see later). In all cases, the reactivation rates ($k_{re\text{-}act}$) are the same, within reasonable error, for H_2 oxidation and H_2 production. Experiments carried out with *Cr*HydA1 and *Ca*HydA showed that $k_{re\text{-}act}$ is strongly light sensitive (see Supporting Information, Figure SI.1) in agreement with earlier electrochemical observations made with *Dd*HydAB.[47] In addition, $k_{re\text{-}act}$ increased significantly when the temperature was raised to 25 °C. From the ratio of rate constants for the reactivation and inactivation reactions at 10 °C, we derived the kinetic inhibition constants $K_I^{CO}(kin) = k_{re\text{-}act}/k_{inact}$. In Table 2, K_I^{CO}(kin) values are compared with the equilibrium values, K_I^{CO}(equil), obtained by titration for *Cr*HydA1 and *Ca*HydA. The two values for *Cr*HydA1 are in good agreement, although for *Ca*HydA, K_I^{CO}(equil) is rather higher than K_I^{CO}(kin). The ratio of the k_{inact} values for CO inhibition of H_2 oxidation and H_2 production—the "catalytic direction discrimination"- is about 49 for *Dd*HydAB, 22 for *Cr*HydA1 and 3 for *Ca*HydA: these variations clearly arise from differences in the rate that CO binds because $k_{re\text{-}act}$ is similar for all three enzymes.

Reactions with O_2. Figure 6 shows experiments in which each enzyme is subjected to 5% O_2 during H_2 oxidation at −0.05 V vs SHE. As before, the H_2 concentration was kept constant throughout the entire time-course. Each experiment began with 80% H_2, 20% N_2 flushing through the cell headspace. The gas mixture was then switched to 80% H_2, 15% N_2, 5% O_2 for the duration of the reaction (this involved simultaneous injection of an aliquot of gas-equilibrated buffer for *Dd*HydAB and *Cr*HydA1; the kinetics of O_2 inactivation of *Ca*HydA were so slow that the injection was unnecessary). The gas was finally changed back to 80% H_2, 20% N_2 once most of the activity (>90%) had been eliminated. We noted that the rate of inactivation by O_2 showed a dependence on H_2 concentration, with inactivation occurring more rapidly at lower levels, thus

Table 2. Compilation of k_{inact} and $k_{re\text{-}act}$ Values for CO Inhibition of H_2 Production and H_2 Oxidation for *Dd*HydAB, *Cr*HydA1 and *Ca*HydA, with the Corresponding Catalytic Direction Discrimination Factors and Values of K_I^{CO} Determined by Kinetic and Equilibrium Methods[a]

	*Dd*HydAB	*Cr*HydA1	*Ca*HydA
H_2 oxidation $k_{inact}/s^{-1}\mu M^{-1}$	3.9×10^{-1} $\pm 3 \times 10^{-1}$	1.9×10^{-2} $\pm 1 \times 10^{-2}$	1.1×10^{-3} $\pm 7 \times 10^{-4}$
H_2 production $k_{inact}/s^{-1}\mu M^{-1}$	8.0×10^{-3} $\pm 7 \times 10^{-3}$	8.4×10^{-4} $\pm 2 \times 10^{-4}$	3.6×10^{-4} $\pm 1 \times 10^{-4}$
Catalytic direction discrimination	49	22	3
H_2 oxidation $k_{re\text{-}act}/s^{-1}$	1.9×10^{-3} $\pm 2 \times 10^{-4}$	2.3×10^{-3} $\pm 1 \times 10^{-3}$	1.8×10^{-3} $\pm 1 \times 10^{-3}$
H_2 production $k_{re\text{-}act}/s^{-1}$	2.7×10^{-3} $\pm 1 \times 10^{-3}$	1.2×10^{-3} $\pm 3 \times 10^{-3}$	2×10^{-3} $\pm 2 \times 10^{-4}$
K_I^{CO} (equil)/μM for H_2 oxidation (at -0.05 V)	–	1.0×10^{-1}	2.2×10^{-1}
K_I^{CO} (kin)/μM for H_2 oxidation (at -0.05 V)	4.8×10^{-3}	1.2×10^{-1}	1.6
K_I^{CO} (kin)/μM for H_2 production (at -0.40 V)	0.34	1.4	5.6

[a] All values pertaining to H_2 production were measured at -0.40 V.

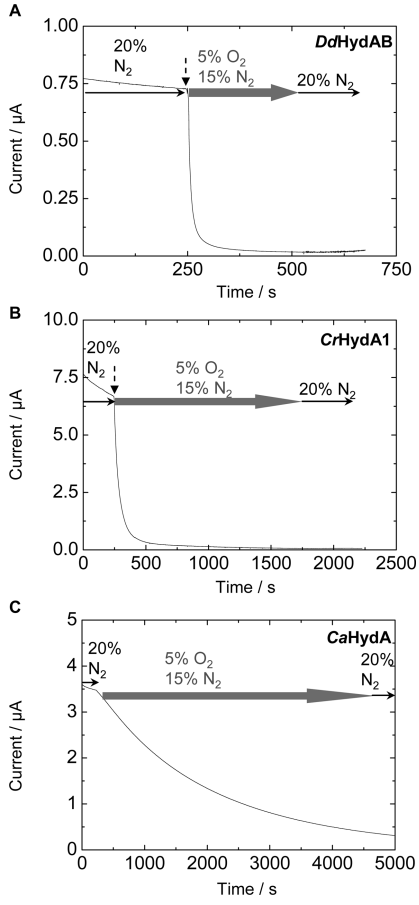

Figure 6. Inactivation of H_2 oxidation by *Dd*HydAB, *Cr*HydA1 and *Ca*HydA by 5% O_2. The headspace mixture is composed of 80% H_2 and the remaining 20% is as indicated. For *Dd*HydAB and *Cr*HydA1 a 0.67 mL aliquot of 20% O_2/80% H_2-saturated buffer was injected into the cell which initially contained 2 mL of buffer, to give an instant concentration of 5% O_2 at the points marked by the dashed arrows. For *Ca*HydA, the reaction was sufficiently slow that it could be initiated simply by changing the headgas mixture. Other conditions: pH 6.0, 10 °C, electrode rotation 3000 rpm, -0.05 V.

indicating that O_2 and H_2 are competitive.[34] We also noted that after removing O_2 from the cell, a very small amount of activity was consistently recovered for all three enzymes. Oxygen

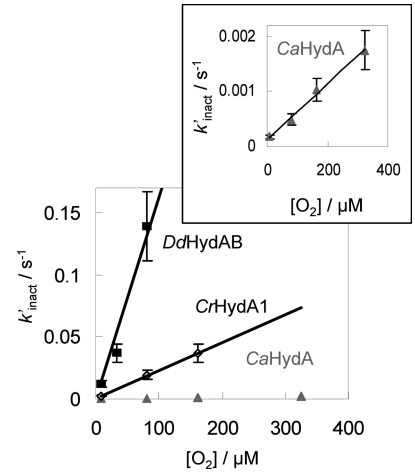

Figure 7. Dependence of rate constants (k'_{inact}) for inactivation of enzymatic H_2 oxidation by O_2, on O_2 concentration, for *Dd*HydAB, *Cr*HydA1 and *Ca*HydA (shown as an expanded scale). Experimental conditions: pH 6.0, 10 °C, electrode rotation 3000 rpm, -0.05 V vs SHE, headspace gas mixture composed of 80% H_2, 20% mixture of N_2 and O_2.

undergoes very slow reduction at graphite at -0.05 V, therefore control experiments (Figure SI.4, Supporting Information) were performed to assess the contribution to the current from O_2 reduction. This contribution to the current was then subtracted from the experiments to verify the end point and the activity remaining. In separate anaerobic experiments we determined that small quantities of hydrogen peroxide that would be formed during electrodic O_2 reduction did not cause inactivation, by injecting aliquots of H_2O_2 solution and monitoring the effect on the H_2 oxidation current at -0.05 V (10 °C). This decrease in current was observed to be much slower than that due to equivalent concentrations of O_2 for all three enzymes.

Figure 7 shows how rate constants for O_2-inactivation of H_2 oxidation activity vary with O_2 concentration for all three [FeFe]-hydrogenases. In each case the rate of inactivation is first-order in O_2 concentration. Table 3 shows the rate constants for inactivation by O_2 alongside the rate constants for inhibition of H_2 oxidation by CO. For each enzyme, the rate of reaction with CO is much faster (80−200-fold) than with O_2 and this ratio, which we refer to as the "gas identity discrimination", is also included in Table 3.

Table 3. Comparison of the Second-Order Rate Constants for Inhibition by CO ($k_{inact}(CO)$) and Inactivation by O_2 ($k_{inact}(O_2)$) of *Dd*HydAB, *Cr*HydA1 and *Ca*HydA and Evaluation of the *Gas Identity Discrimination*—the Ratio $k_{inact}(CO)/k_{inact}(O_2)$

enzyme	$k_{inact}(CO)/s^{-1}\mu M^{-1}$	$k_{inact}(O_2)/s^{-1}\mu M^{-1}$	$k_{inact}(CO)/k_{inact}(O_2)$
*Dd*HydAB	3.9×10^{-1}	$1.8 \times 10^{-3} \pm 3 \times 10^{-4}$	217
*Cr*HydA1	1.9×10^{-2}	$2.2 \times 10^{-4} \pm 1 \times 10^{-4}$	86
*Ca*HydA	1.1×10^{-3}	$5.1 \times 10^{-6} \pm 1 \times 10^{-6}$	216

H_2 Production in the Presence of O_2. Finally, we carried out experiments to estimate the extent to which the rate of inactivation by O_2 depends on whether the hydrogenase is operating in the direction of H_2 production or H_2 oxidation. We used a procedure described recently,[44] in which the problem of distinguishing the current due to enzymatic H^+ reduction from that due to electrochemical O_2 reduction is resolved by adding an inhibitor. The decrease in current observed when the inhibitor is added provides a direct measure of the component of the current due to enzyme-catalyzed H^+ reduction. The experiments conducted for *Dd*HydAB, *Cr*HydA1 and *Ca*HydA are shown in Figure 8.

The experiment performed on *Dd*HydAB started under an atmosphere of N_2, and a current corresponding to enzyme-catalyzed H_2 production was recorded (stage 1). The headgas was then switched to 1% CO in N_2, and a rapid and almost complete loss of current was observed. When the CO was flushed from the cell, the current increased and reached a steady level (albeit not the same level as prior to CO introduction, due to the partial irreversibility of this reaction, see Figure 4). The current that was recovered during CO efflux was adopted as the normalization unit for the next stage. In stage 2, O_2 was introduced: the current initially increased due to direct reduction of O_2 at the graphite electrode but then began to decrease as the enzyme became inactivated. Introduction of 1% CO after 2000 s under O_2 resulted in a rapid loss of current, the magnitude of which reports on the enzyme-catalyzed current component prior to CO inhibition. Removal of CO caused the current to increase again, but a further decrease in current was observed, as expected, when O_2 was removed from the cell after $t =$ 8500 s. Finally in stage 3 the inhibition step with CO was repeated to establish the extent of survival of the hydrogenase. Similar sequences of steps were used in the experiments with *Cr*HydA1 and *Ca*HydA, except that 99% and 95% CO, respectively, were used instead of 1% CO in order to compensate for the much slower kinetics and lower CO affinity of these hydrogenases compared to *Dd*HydAB; in addition, 5% O_2 was used to obtain a higher rate of inactivation for *Ca*HydA. To estimate the half-life for inactivation in each case, the decrease in current upon addition of CO after reaction with O_2 for t seconds (during stage 2) was divided by the original increase in current observed when CO was removed during stage 1. The half-life was calculated using $t_{1/2} = -t \ln 2/\ln(x)$ where x is the fraction of H_2 production current surviving after t seconds. From control experiments such as those previously described,[44] it was estimated that the concentrations of O_2 experienced by the enzyme at −0.4 V under headgas conditions of 1% and 5% were 0.7% and 4.5%, respectively. The corresponding half-lives for H_2 oxidation activity under similar O_2 concentrations were calculated from the rate constants in Table 3. The results and comparisons are shown in Table 4.

All enzymes remained at least 30% active after 2000 s under 1% bulk O_2 (i.e., at least 0.7% O_2 at the electrode[44]) for *Dd*HydAB and *Cr*HydA1 and even under 5% bulk O_2 (around 4.5% O_2 at the electrode) for *Ca*HydA. More significantly, there were important differences among the three enzymes when comparing their survival to O_2 exposure

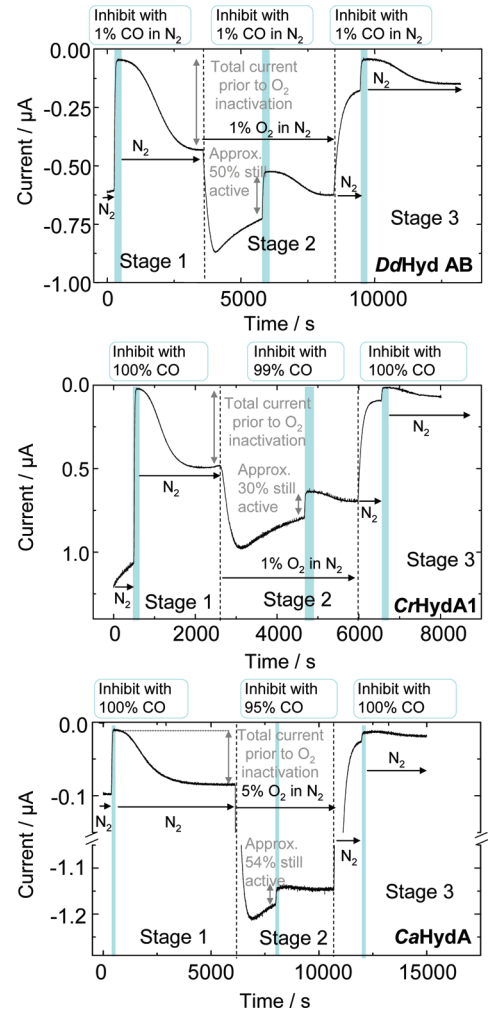

Figure 8. Chronoamperometric experiments designed to measure the survival of H_2 production activity in the presence of headspace levels of 1% O_2 for *Dd*HydAB and *Cr*HydA1, and 5% O_2 for *Ca*HydA (note change in current scale upon introduction of 5% O_2). All procedures were carried out using 1 bar pressure of the gases indicated. Other conditions: pH 6.0, 10 °C, electrode rotation 3000 rpm, −0.4 V vs SHE. The blue vertical lines show introductions of CO to inhibit and reveal enzyme-catalyzed H_2 production. The fraction of enzyme surviving O_2 after time t is given by the ratio of CO-sensitive current measured in Stage 2 relative to that measured after the recovery in Stage 1 (indicated by vertical double-headed arrows in each case).

Table 4. Comparative Half-Lives (s) for O_2-Inactivation of H_2 Production and H_2 Oxidation of *Dd*HydAB, *Cr*HydA1 and *Ca*HydA[a]

catalytic direction	*Dd*HydAB	*Cr*HydA1	*Ca*HydA
H_2 oxidation	30	305	1890
H_2 production	∼2000	∼1320	∼2250
Catalytic direction discrimination	60−70	4−5	approximately 1

[a] The half-lives for the H_2 production reaction are estimated on the basis of the percentage of activity remaining after an extended period (1800−2000 s, different for each enzyme) of catalytic turnover in the presence of O_2. Experimental conditions for H_2 production: *Dd*HydAB, *Cr*HydA1; 1% O_2 in the headgas (i.e. at least 0.7% O_2 surviving at the electrode); *Ca*HydA, 5% O_2 in the headgas (at least 4.5% surviving at the electrode) −0.4 V, pH 6, 10 °C, electrode rotation rate 3000 rpm. Data for H_2 oxidation were calculated using the second-order rate constants (see Table 3) and values of 0.7% O_2 for *Dd*HydAB and *Cr*HydA1; and 4.5% O_2 for *Ca*HydA.

during H_2 production with the data obtained for H_2 oxidation. In the case of *Dd*HydAB, the H_2-production activity remaining is about sixty-fold greater than expected on the basis of the results described above for O_2 inactivation of H_2 oxidation. The enhancement is also observed for *Cr*HydA1, but to a lesser extent than *Dd*HydAB. On the other hand, no clear difference was observed for *Ca*HydA between the rates of inactivation observed when monitoring H_2 production at −0.4 V or H_2 oxidation at −0.05 V.

Discussion

The three hydrogenases we have investigated include two with potential applications in large-scale H_2 production (*Cr*HydA1 for photosynthesis and *Ca*HydA for fermentation) and one of known crystal structure (*Dd*HydAB).[48] In addition, *Ca*HydA is closely related to *Cp*I for which the structure is known.[22,23] Some important comparisons have been made, exploiting the unique ability of protein film electrochemistry to measure, simultaneously, the rates and extent of changes in catalytic activities under well-defined potentials (driving force). A summary of the quantitative observations and interrelationships is provided in Figure 9.

The reactions with CO are highly informative, and we[34] and others[39] have noted that CO protects [FeFe]-hydrogenases against O_2 degradation, suggesting both inhibitors target the same site. In all cases we could use CO as a strong inhibitor of both H_2 oxidation and H_2 production, helped by the fact that binding of H_2 under both conditions is much weaker than CO binding[49] (see Table 1).

Light sensitivity of CO inhibition is a well-established property of [FeFe]-hydrogenases[13,30,33,47,50−53] and originates from the photolability of the Fe-CO bond.[54] A particularly useful result is the similarity in the rates of *dark* reactivation of the CO-inhibited hydrogenases. In all cases, the rate is accelerated by illumination (as reported in an earlier study for *Dd*HydAB[47]), and this suggests strongly that the reaction being observed in all cases is an elementary dissociation of the Fe-CO bond. This result demonstrates an intrinsic property of the H-cluster, maintained regardless of the slightly differing protein environments among the [FeFe]-hydrogenases. Evidently, all that is required for reactivation is to liberate the coordination site and ensure that CO escapes from the pocket before it can recombine.[30]

Our K_I^{CO} data for *Ca*HydA determined during H_2 oxidation lie broadly in the range of values (around 1 μM) obtained by Thauer and co-workers[50] for CO binding to the related enzyme from *C. pasteurianum*, although those experiments also used a higher temperature and we found a consistently higher value

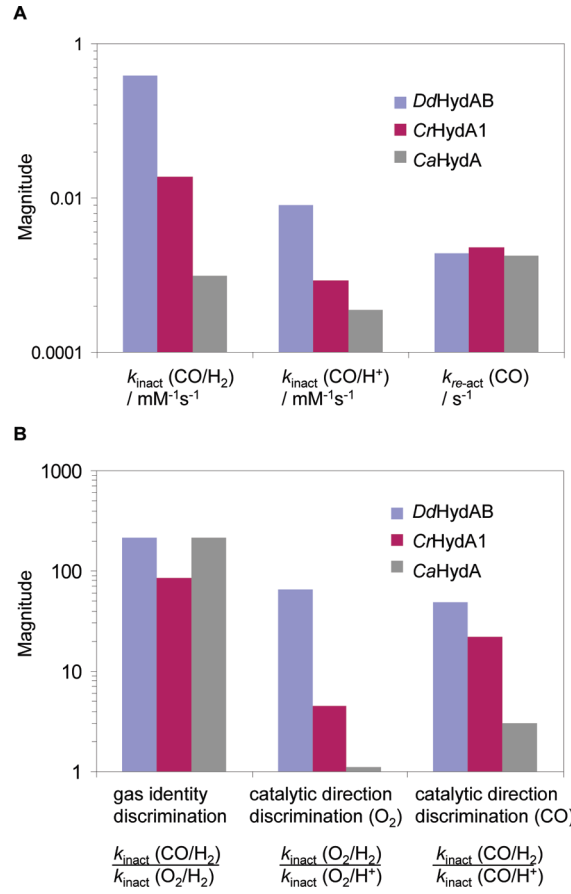

Figure 9. Bar charts representing various comparisons between *Dd*HydAB, *Cr*HydA1, and *Ca*HydA. (A) Comparative rates of CO-inhibition of H_2 oxidation ($k_{inact}(CO/H_2)$), H^+ reduction ($k_{inact}(CO/H^+)$) and rates of recovery from CO-inhibition ($k_{re\text{-}act}(CO)$). (B) Discrimination factors characterizing the favorability of binding CO over O_2 ($k_{inact}(CO/H_2)/k_{inact}(O_2/H_2)$), binding O_2 when the enzyme is catalyzing H_2 oxidation compared to H_2 production ($k_{inact}(O_2/H_2)/k_{inact}(O_2/H^+)$) and binding CO when the enzyme is catalyzing H_2 oxidation compared to H_2 production ($k_{inact}(CO/H_2)/k_{inact}(CO/H^+)$) for *Dd*HydAB, *Cr*HydA1 and *Ca*HydA. As the rate of reactivation from CO inhibition is essentially independent of the process being catalyzed, it is simply represented by the term $k_{re\text{-}act}(CO)$. The $k_{inact}(O_2/H_2)/k_{inact}(O_2/H^+)$ ratios are approximate because the values of $k_{inact}(O_2/H^+)$ are estimates. This ratio is approximated to 1 for *Ca*HydA.

(weaker binding) for the kinetic compared to the equilibrium value. The reasons for this are unclear at present, and doubtless the model we now discuss is oversimplified. The rate data for all three enzymes, both qualitative (Figure 3) and quantitative (Figure 4 and Figure 5), reveal a preference for CO binding to the enzymes under H_2 oxidation—the direction enforced by a higher electrode potential that should ensure that H_{ox} predominates over H_{red} during the catalytic cycle. The "catalytic direction discrimination" for CO decreases in the order *Dd*HydAB > *Cr*HydA1 ≫ *Ca*HydA—the same order as found for the equivalent factor estimated for O_2 inactivation. The order also matches that observed for the rates of inactivation of H_2 oxidation by CO and O_2. These interrelationships lead us to propose a model for the *reversible* binding of CO to [FeFe]-hydrogenases which can be extended to account for reactions with O_2. The model is represented schematically in Figure 10A.

The model considers that the attack by CO (rate constant k_{inact}) involves two stages: the first stage is transport of CO (we treat this generically as the small molecule X) from the external medium (X_{ext}) through the enzyme (for simplicity we show this as a single tunnel without branches or sites at which X could

(48) Nicolet, Y.; Piras, C.; Legrand, P.; Hatchikian, C. E.; Fontecilla-Camps, J. C. *Struct. Folding Des.* **1999**, *7*, 13–23.
(49) This allowed for the same concentration of H_2 to be employed in the experiments at −0.4 and −0.05 V, thus ensuring that the experiments were comparable. For other hydrogenases, strong H_2 inhibition of H_2 production at −0.4 V would have prevented experiments performed at this potential from being performed under 80% H_2 as they were at −0.05 V.
(50) Thauer, R. K.; Kaufer, B.; Zahringe, M.; Jungerma, K. *Eur. J. Biochem.* **1974**, *42*, 447–452.
(51) Purec, L.; Krasna, A. I.; Rittenberg, D. *Biochemistry* **1962**, *1*, 270–275.
(52) Kempner, W.; Kubowitz, F. *Biochem. Z.* **1933**, *257*, 245.
(53) Albracht, S. P. J.; Roseboom, W.; Hatchikian, E. C. *J. Biol. Inorg. Chem.* **2006**, *11*, 88–101.
(54) Kochanski, E. *Photoprocesses in Transition Metal Complexes, Biosystems and Other Molecules: Experimental and Theory*; Kluwer Academic Press: London, 1992.

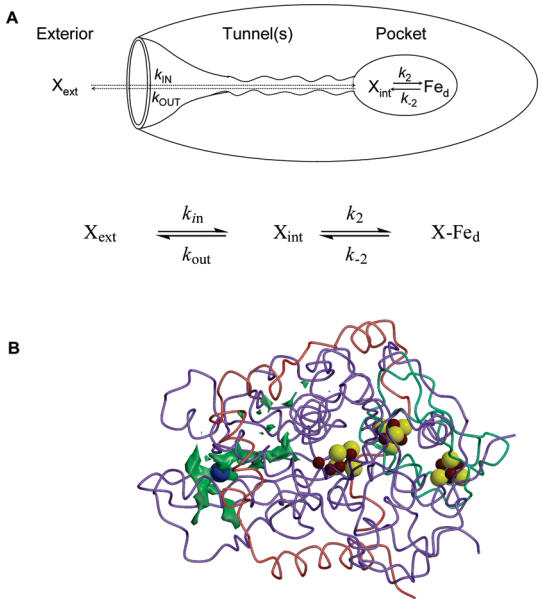

Figure 10. (A) Cartoon depicting the stepwise reaction of an inhibitory gas molecule X (= CO) with the buried H-cluster (Fe_d) of a [FeFe]-hydrogenase, showing transfer from the external medium (X_{ext}) to a position (X_{int}) close to Fe_d (k_{in}, k_{out}), and inner-sphere coordination/dissociation at Fe_d (k_2, k_2). (B) C-α tracing of the [FeFe]-hydrogenase from *D. desulfuricans*: *Dd*HydAB(large subunit: blue and green, small subunit: red) and the cavity observed in the crystals (probe size: 0.8 Å, program CAVsel, A. Volbeda, unpublished). The H-cluster occupies the center of the molecule. The blue sphere represents the experimentally observed Xe site. Other color codes: red: Fe, yellow: S.

be trapped) to a noncoordinating site close to the H-cluster; the second stage is migration of X_{int} from the noncoordinating site to a coordination site that we assume to be Fe_d (the actual inner-sphere binding reaction). The process of reactivation (overall rate constant $k_{re\text{-}act}$) is the reverse of this reaction scheme.

The terms k_{in} and k_{out} are rates of transport of X through the protein in either direction, and k_2 and k_{-2} are the elementary rates of binding and dissociation of ligand X, respectively, to Fe_d within the region of the active-site pocket. With the simplification that k_{-2}[X-Fe_d] is negligible until the reaction of inhibitor with enzyme is essentially complete, the steady-state approximation with $d[X_{int}]/dt = 0$ yields:

$$\text{rate of inactivation} = \frac{k_{in}k_2[X_{ext}][Fe_d]}{k_{out} + k_2} \tag{3a}$$

where the pseudo first-order rate constant (as measured directly in experiments) is:

$$k'_{inact} = \frac{k_{in}k_2[X_{ext}]}{k_{out} + k_2} \tag{3b}$$

An assumption of this model is that k_{in} and k_{out} should depend on the nature of the gas molecule and gas filter but not on the catalytic state of the H-cluster—the state predominating for a particular electrode potential, i.e. H_{ox} or H_{red}. Based on the evidence that CO binds preferentially (and perhaps exclusively) to H_{ox},[29] we expect that k_2 for CO will be large for H_{ox} and small, even zero, for H_{red}. Note however that inhibition is still observed during H_2 production because H_{ox} may always appear briefly in the catalytic cycle, even at the lowest potentials we have used (−600 mV in the cyclic voltammetry experiments).

Recognizing this is a simplistic model, we now consider the following limiting scenarios: (i) if $k_{out} \leq k_2$, $k'_{inact} \sim k_{in}[X_{ext}]$ so the rate of inhibitor binding depends only on the external concentration and rate of internal transport of X; in this case little discrimination is expected based on the redox state of the H-cluster. Alternatively, (ii), if $k_{out} \gg k_2$, i.e. if the protein's internal structure does not provide an effective barrier to transport of X, it follows that $k'_{inact} = k_2k_{in}[X_{ext}]/k_{out}$. In this scenario, the rate of inhibition depends not only on the nature of X but also upon k_2 and therefore should also be faster for conditions favoring H_{ox} (H_2 oxidation) compared to H_{red} (H_2 production).

Reactivation follows the reverse sequence, and for $k_{in}[X_{ext}] = 0$ (because CO is removed from the solution) we obtain

$$\text{rate of re-activation} = \frac{k_{out}k_{-2}[\text{X-Fe}_d]}{k_{out} + k_2} \tag{4a}$$

and the first-order rate constant (as measured experimentally) is given by

$$k_{re\text{-}act} = \frac{k_{out}k_{-2}}{k_{out} + k_2} \tag{4b}$$

Under the limiting condition $k_{out} \ll k_2$, $k_{re\text{-}act} = k_{out}k_{-2}/k_2$, whereas if $k_{out} \gg k_2$, the rate of reactivation reduces to k_{-2}, reflecting the likelihood that CO escapes from the enzyme (k_{out}) before it can recoordinate (k_2). Our data suggest that the latter situation must generally be the case, with a more intermediate situation (a smaller k_{out} relative to k_2) applying for *Ca*HydA (see below). Overall, the dissociation constant is given by $K_I^{CO}(\text{kin}) = k_{re\text{-}act}/k_{inact} = k_{out}k_{-2}/k_{in}k_2$, which always depends on the kinetics of making and breaking the Fe-CO bond.

This analysis can be extended to the reaction of [FeFe]-hydrogenases with O_2, although that reaction is essentially irreversible. Table 3 and Figure 9 show that trends among the hydrogenases as observed for their reactions with CO are mirrored in their reactions with O_2; for example, *Dd*HydAB shows the highest rates of inhibition in both cases and the greatest discrimination based on catalytic direction.

In mechanistic terms, the minuscule protection that *Dd*HydAB possesses against attack by O_2 is provided only within the active-site pocket in which O_2 is able to discriminate between different catalytic states of the enzyme (a strong k_2 dependence, according to the model). In contrast, the small catalytic direction discrimination observed for *Ca*HydA can be interpreted in terms of it showing a less excessive value of k_{out} (a more restrictive tunnel or filter) in relation to k_2. Values for k_{out} should correlate closely with those for k_{in};thus, it is significant that *Ca*HydA also shows the slowest rates of reaction with CO and O_2 and, with a half-life of several minutes under atmospheric O_2 levels at 10 °C, looks to be a promising model for aerobic biohydrogen production even though it stems from a strict anaerobe.

The evidence (strong light enhancement) that the rate-determining step in reactivation is the elementary scission of the Fe-CO bond in the H_{ox}-CO state, and the observation that the rate measured in the dark is quite similar for all enzymes (which share only 40% sequence similarity) shows that the kinetics of reactivation are governed more by the intrinsic properties of the H-cluster than by the nature of the surrounding enzyme. Lubitz and colleagues have proposed that the H-clusters in *Cr*HydA1 and *Dd*HydAB are similar, although they differ slightly in electronic detail.[28] Note that were CO to coordinate

to different states of the H-cluster at −0.4 and −0.05 V, we would expect $k_{re\text{-}act}$ to depend significantly on potential, but it does not. This supports the view that CO (and by extension, O_2) binds to H_{ox} but not H_{red}. The other comparison in Figure 9 which is reasonably constant among all three enzymes is the gas identity discrimination (CO vs O_2). This again may reflect intrinsic behavior of the H-cluster because CO is a superior ligand to O_2 in terms of its π-acceptor capability. Dominant intrinsic effects are not unexpected, given the unusually independent status of the $2Fe_H$ subcluster, which was described in the Introduction as an enzyme cofactor resembling an organometallic compound buried in a protein. Clearly our model is an oversimplification, albeit necessary at this stage, and to understand this observation more fully we are undertaking theoretical calculations, including predictions of relative transport rates through the enzyme.

The notion of a filter or a tunnel connecting the H-cluster to the molecular surface is supported by the two available [FeFe]-hydrogenase structures. In *Dd*HydAB and *Cp*I there is a 'static' tunnel that can be revealed using a cavity-searching program.[55] The tunnel in each enzyme has a central cavity that can bind a Xe atom and a narrower path leading to Fe_d.[17,26] Figure 10B depicts the experimentally observed tunnel and Xe site in *Dd*HydAB.[56,57] The tunnel connects the molecular surface to the active site, and one possibility is that the Xe atom occupies a cavity in which dissociated CO could reside before rebinding to Fe_d or escaping to the medium. Molecular dynamics simulations based upon the *Cp*I structure revealed a second tunnel that also connects to the central cavity.[58] What can be concluded from both crystallographic and theoretical studies is that dynamic fluctuations are important for intramolecular gas diffusion in [FeFe]-hydrogenases.

Two further mechanistic points emerge from this study. First, we always observed that CO inhibition of H_2 production is only partially reversible. At present we have no explanation for this, although Adams reported in 1987 that CO binds irreversibly to a catalytic intermediate of *Cp*I.[59] Further investigations including a full study of the potential dependence of CO binding during H_2 production are clearly required to resolve this issue, which may have mechanistic relevance. Second, we always recorded a small proportion of activity returning after O_2 inactivation, an observation in line with those reported by Baffert et al.[39] also in studies on *Ca*HydA. Such a part-reversal is consistent with the mechanism proposed by Stripp et al.[34] in which O_2 must first bind in a reversible manner at the distal Fe of the $2Fe_H$ subcluster before causing irreversible damage to the $[4Fe\text{-}4S]_H$ subcluster.

From a biological perspective, the precise, quantitative data that we have been able to extract and compare for the three different hydrogenases should be understandable in terms of the lifestyles of the organisms that express them. This is true, in part. Recent studies on the O_2 detoxification mechanism in *C. acetobutylicum* have shown that this fermentative bacterium can survive limited exposure to air and can even undergo cell division at surprisingly high concentrations of O_2.[60,61] The relative O_2 stability of *Ca*HydA may therefore be a consequence of concerted evolutionary adaptation to an O_2-rich atmosphere. However, certain species of the *Desulfovibrio* genus have also been reported to exhibit short-term survival when exposed to O_2;[62,63] thus, from a microbiological viewpoint the large disparity in O_2 sensitivity between *Ca*HydA and *Dd*HydAB is puzzling. The 'intermediate' degree of O_2 sensitivity displayed by *Cr*HydA1 is consistent with the observation that although it is only expressed in *C. reinhardtii* under anaerobiosis[64,65] it is likely to be in contact with at least trace amounts of O_2 that are produced by photosystem II.[66]

Acknowledgment. Research in the group of FAA was supported by the UK BBSRC (Grant BB/D52222X) and EPSRC. C.C. and J.C.F.C. thank the CEA and the CNRS (France) for institutional funding. S.S. and T.H. were supported by the Deutsche Forschungsgemeinschaft (SFB 480) and EU/Energy Network SolarH2 (FP7 418 contract 212508. We thank Dr. Alison Parkin for providing part of Figure 3 and for helpful advice, and Dr. A. Volbeda for preparing Figure 10B.

Supporting Information Available: Photolability of the CO-bound state; determination of the variation of the concentration of CO with time in the experiments shown in Figure 4; determination of K_I^{CO}(equil); control experiments for experiments investigating O_2 inactivation of H_2 oxidation. This material is available free of charge via the Internet at http://pubs.acs.org.

JA905388J

(55) Montet, Y.; Amara, P.; Volbeda, A.; Vernede, X.; Hatchikian, E. C.; Field, M. J.; Frey, M.; Fontecilla-Camps, J. C. *Nat. Struct. Biol.* **1997**, *4*, 523–526.
(56) Fontecilla-Camps, J. C.; Amara, P.; Cavazza, C.; Nicolet, Y.; Volbeda, A. *Nature* **2009**, *460*, 814–822.
(57) Nicolet, Y.; Piras, C.; Legrand, P.; Hatchikian, C. E.; Fontecilla-Camps, J. C. *Structure* **1999**, *7*, 13–23.
(58) Cohen, J.; Kim, K.; Posewitz, M.; Ghirardi, M. L.; Schulten, K.; Seibert, M.; King, P. *Biochem. Soc. Trans.* **2005**, *33*, 80–82.
(59) Adams, M. W. W. *J. Biol. Chem.* **1987**, *262*, 15054–15061.
(60) Hillmann, F.; Fischer, R. J.; Saint-Prix, F.; Girbal, L.; Bahl, H. *Mol. Microbiol.* **2008**, *68*, 848–860.
(61) May, A.; Hillmann, F.; Riebe, O.; Fischer, R. M.; Bahl, H. *FEMS Microbiol. Lett.* **2004**, *238*, 249–254.
(62) Cypionka, H. *Annu. Rev. Microbiol.* **2000**, *54*, 827–848.
(63) Lumppio, H. L.; Shenvi, N. V.; Summers, A. O.; Voordouw, G.; Kurtz, D. M. *J. Bacteriol.* **2001**, *183*, 2970–2970.
(64) Happe, T.; Naber, J. D. *Eur. J. Biochem.* **1993**, *214*, 475–481.
(65) Happe, T.; Kaminski, A. *Eur. J. Biochem.* **2002**, *269*, 1022–1032.
(66) Happe, T.; Hemschemeier, A.; Winkler, M.; Kaminski, A. *Trends Plant Sci.* **2002**, *7*, 246–250.